Thermodynamic, electronic and structural properties of Cu/CeO 2 surfaces and interfaces from first-principles DFTU calculations

ARTICLE *in* THE JOURNAL OF CHEMICAL PHYSICS · DECEMBER 2010

Impact Factor: 2.95 · DOI: 10.1063/1.3515424 · Source: PubMed

5 AUTHORS, INCLUDING:

Lucie Szabova
National Institute for Materials Science
6 PUBLICATIONS **63** CITATIONS
SEE PROFILE

Matteo Farnesi Camellone
Italian National Research Council
23 PUBLICATIONS **391** CITATIONS
SEE PROFILE

Vladimir Matolin
Charles University in Prague
285 PUBLICATIONS **3,013** CITATIONS
SEE PROFILE

Stefano Fabris
Italian National Research Council
75 PUBLICATIONS **6,247** CITATIONS
SEE PROFILE

Thermodynamic, electronic and structural properties of Cu/CeO_2 surfaces and interfaces from first-principles DFT+U calculations

Lucie Szabová,[1] Matteo Farnesi Camellone,[2,a)] Min Huang,[2,b)] Vladimír Matolín,[1] and Stefano Fabris[2,3,c)]

[1]*Department of Surface and Plasma Science, Faculty of Mathematics and Physics, Charles University, V Holešovičkách 2, 18000 Prague 8, Czech Republic*

[2]*CNR-IOM DEMOCRITOS, Theory@Elettra group, Istituto Officina dei Materiali, Area Science Park, I-34149 Basovizza, Trieste, Italy*

[3]*SISSA - Scuola Internazionale Superiore di Studi Avanzati and Italian Institute of Technology (IIT-SISSA Unit), via Bonomea 265, I-34136 Trieste, Italy*

(Received 21 August 2010; accepted 22 October 2010; published online 20 December 2010)

The thermodynamic, structural and electronic properties of Cu–CeO_2 (ceria) surfaces and interfaces are investigated by means of density functional theory (DFT+U) calculations. We focus on model systems consisting of Cu atoms (i) supported by stoichiometric and reduced CeO_2 (111) surfaces, (ii) dispersed as substitutional solid solution at the same surface, as well as on (iii) the extended $Cu(111)/CeO_2(111)$ interface. Extensive charge reorganization at the metal–oxide contact is predicted for ceria-supported Cu adatoms and nanoparticles, leading to Cu oxidation, ceria reduction, and interfacial Ce^{3+} ions. The calculated thermodynamics predict that Cu adatoms on stoichiometric surfaces are more stable than on O vacancies of reduced surfaces at all temperatures and pressures relevant for catalytic applications, even in extremely reducing chemical environments. This suggests that supported Cu nanoparticles do not nucleate at surface O vacancies of the oxide, at variance with many other metal/ceria systems. In oxidizing conditions, the solid solutions are shown to be more stable than the supported systems. Substitutional Cu ions form characteristic CuO_4 units. These promote an easy and reversible O release without the reduction of Ce ions. The study of the extended $CeO_2(111)/Cu(111)$ interface predicts the full reduction of the interfacial ceria trilayer. Cu nanoparticles supported by ceria are proposed to lie above a subsurface layer of Ce^{3+} ions that extends up to the perimeter of the metal–oxide interface. © *2010 American Institute of Physics*. [doi:10.1063/1.3515424]

I. INTRODUCTION

Environment protection and sustainable energy storage/conversion strongly rely on the development of novel more reactive and stable catalysts.[1] Catalytic converters for gas exhausts in the automotive industry or electrodes for fuel cells are representative examples in this context. Some of the most efficient of these catalysts comprised of metal particles supported by metal oxides. On the one hand, the activity of the supported catalysts is determined by the specific electronic and structural properties of the individual constituents (i.e., the oxide support and the metal nanoparticles). On the other hand, the reactivity is also correlated to the charge state of the metal nanoparticles that is controlled by electronic charge transfer effects arising at the metal/oxide interface, which are the subject of the present paper.

Reducible oxides, and in particular cerium oxide (CeO_2 or ceria), have been shown to be active supports for the activation and stability of supported metal particles as well as for reversible oxygen exchange during reaction.[2–4] In particular, copper–ceria catalysts promote CO oxidation,[5–7] NO reduction,[8,9] water–gas shift,[10] and methanol steam reforming.[11] Similarly to the case of other metal–ceria systems,[12–16] also the reactivity of copper–ceria catalysts has been proposed to be enhanced by surface ionic metal species. Materials exposing surface Cu^+ or dispersed Cu^{2+} ionic species have been reported in the literature, the presence of the one or the other being determined by the synthesis conditions.[5,17] To our knowledge, negatively charged supported Cu species were instead never reported. This is an important and distinctive difference with respect to Au, where metal clusters are known to nucleate from negatively charged $Au^{\delta-}$ species on O vacancies of the oxide support.[14,15,18,19] Identifying a clear correlation between the charge state of Cu adsorbates with the stoichiometry of the ceria support is one of the goals of the present paper.

The high reactivity of copper–ceria catalysts motivated several experimental analysis focused on identifying the chemical and electronic effects arising from the interaction at the interface and leading to the improved catalytic properties. In particular, the valence band states of copper-loaded ceria powder consisting of submicrometer ceria particles covered with thin copper film were studied by means of x-ray and synchrotron radiation photoemission spectroscopies

a)Present address: Lehrstuhl für Theoretische Chemie, Ruhr–Universität Bochum, 44780 Bochum, Germany.

b)Present address: Department of Materials Science and Engineering and Department of Physics, The University of Texas at Dallas, Richardson, Texas 75080, USA.

c)Author to whom correspondence should be addressed. Electronic mail: fabris@sissa.it.

(XPS and SRPES).[20] The effect of the copper/ceria interface was then specifically addressed by means of the inverse model system consisting of two monolayers of ceria grown on a copper (111) surface plane. Both systems exhibited higher activity toward CO oxidation.[20] The importance of studying inverse model Cu/ceria systems consisting of ceria nanoparticles on copper surface was analyzed in Ref. 21. These studies demonstrated that in both cases [ceria powders[22] and extended (111) surface[23]] the interaction with Cu lead to partial reduction of the oxide. The inverse CeO_2/CuO catalysts were also the subject of a recent study addressing the water–gas-shift reaction.[17] This inverse CeO_2/CuO–Cu catalyst displayed a higher reactivity than standard Cu/CeO_2 systems. Also in this case, the substrate was shown to be reduced by the contact with the metal. In addition, during reaction, the CuO was shown to transform to metallic Cu via a Cu_2O intermediate, thus suggesting oxidation states of the Cu ranging from II to 0. In order to rationalize the reported experimental data and the proposed physical interpretations, we analyze in this paper the interfaces between model ceria (111) surfaces and various Cu systems, from adatoms to extended metal surfaces, by means of density functional theory (DFT) calculations.

It is by now well established that standard energy functionals available for DFT calculations do not allow for a reliable description of reduced ceria, i.e., when an electron is localized on the Ce-4f states leading to a Ce^{3+} ion.[24–28] The problem lies in the limited ability of the standard functionals in correctly capturing the self-interaction correction. There are several studies on the structural properties of ceria employing these standard DFT approaches, either with the local density approximation (LDA) or the generalized gradient approximation (GGA) (Refs. 26, 29–34, and 35) for the exchange and correlation functional. These and other computational studies allowed to explore the predictive power of the LDA and GGA,[31,34–38] which resulted to be rather limited when dealing with reduced ceria. The addition of a Hubbard U term to the energy functional (DFT+U method) that accounts for the on-site Coulomb interaction, turns out to allow for capturing in a semi-quantitative way the structural and electronic properties of stoichiometric and reduced bulk ceria[24–28] as well as of its most stable surfaces, also in the presence of molecular adsorbates[39–41] and metal adatoms.[42–45] This DFT+U approach has recently become very popular for the numerical simulation of ceria-based materials and has been shown to give substantially similar results to those obtained with hybrid functionals.[46]

Very recently two computational analyses addressed the Cu–CeO_2 system with DFT+U methods.[47,48] Branda *et al.*[47] studied the case of the Cu adsorption on the stoichiometric surface comparing the results obtained for Ag and Au adsorbates. Yang *et al.*[48] instead focused on the issue of CO adsorption and oxidation on Cu atoms dispersed into the ceria lattice, showing that their presence favor the adsorption of CO on the CeO_2 surface, similarly to what was previously reported for Au adatoms.[44,49]

Our study stems from these works. We first present a complete and unified description of Cu adatoms supported on stoichiometric and defective CeO_2(111) surfaces, as well as dispersed as substitutional point defects in surface solid solutions. We then extend these results by studying the relative stability of these surface structures (in terms of their free energy of formation) including the effect of the chemical environment (temperature and partial pressure of O_2). This analysis shows that larger Cu nanoparticles are supported by stoichiometric CeO_2 surfaces even in reducing conditions, thus ruling out the presence of O vacancies at the metal–oxide interface. This leads to the final part of our work, where we analyse the extended interface between a supported Cu nanoparticle and the ceria surface, by focusing on the coherent Cu(111)/CeO_2(111) interface.

II. METHOD

Our calculations were based on the density functional theory employing the GGA approximation for the exchange-correlation functional in the formulation of Perdew–Burke–Ernzerhof.[50] As noted above, a reliable description of both stoichiometric and reduced ceria based materials can be achieved by adding a Hubbard U term to the GGA energy functional acting on the f states of the Ce ions. All the calculations presented in this work were performed at the DFT+U level, in the implementation of Cococcioni and de Gironcoli[51] together with a value of the parameter U of 4.5 eV. This is consistent with our previous works and agrees with the current literature reporting values between 4.5 and 5 eV.[25–28,39,42,43,46] In order to assess the dependency of the main results on this parameter, selected calculations were performed with different values of U in the range (2.5–4.5). The system wave function was represented by a basis set of plane waves limited by an energy cutoff of 30 Ry, while the cutoff for the electron density representation was set to 300 Ry. The interaction between the valence electrons and the ions was described by means of ultrasoft pseudopotentials.[52] In the study of supported and dispersed Cu atoms, integrals in the Brillouin zone were performed on a Monkhorst–Pack (4 × 4 × 1) k-point mesh and a smearing of 0.005 Ry. A (4 × 4 × 2) mesh was used for the study of the extended metal–oxide interface, together with a Methfessel–Paxton smearing of 0.02 Ry. Both values for the cut off parameters and the mesh for the k-points were determined in preliminary tests performed to ensure sufficient convergence of the results.[53] All calculations were spin polarized and were carried out with the PWscf code of the Quantum EXPRESSO package.[54]

Bonding charge density analysis was performed by calculating the charge difference $\Delta\rho = \rho_{CeO_2/Cu} - (\rho_{CeO_2} + \rho_{Cu})$, between the density of the complete system ($\rho_{CeO_2/Cu}$) and the densities of the isolated noninteracting systems of a copper atom (ρ_{Cu}) and ceria surface (ρ_{CeO_2}).

A. Surface structures involving Cu adatoms and CeO_2(111)

The adsorption and solid solutions of Cu adatoms on (in) the (111) ceria surface were modeled by orthorhombic (2 ×2) computational supercells comprising three CeO_2 trilayers in the following sequence O–Ce–O–O–Ce–O–O–Ce–O. The two oxygen-terminated surfaces on each side of the ceria slab were separated by 11 Å thick vacuum layer.

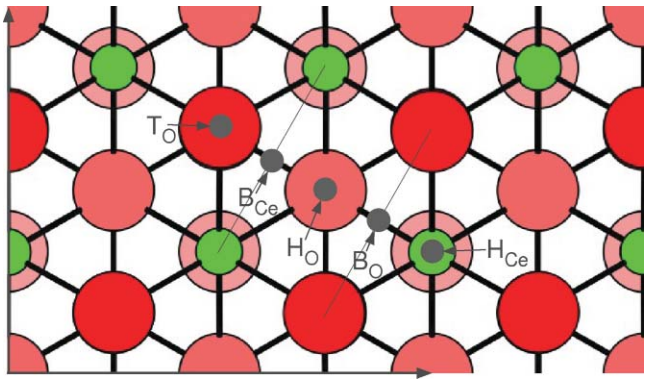

FIG. 1. Top view of the $CeO_2(111)$ surface. Surface and subsurface O atoms are represented by dark (red) and light (pink) large circles ... while Ce ions are displayed as light (green) small circles.. The gray dots indicate the high-symmetry initial sites for the adsorption of a Cu adatom investigated in this study.

The lowest energy adsorption configuration of a Cu adatom on the stoichiometric ceria (111) surface was determined by exploring the five high-symmetry surface sites displayed in Fig. 1. For the stoichiometric surface, we considered the sites on top of an O atom (T_O), the bridge between two Ce atoms (B_{Ce}), the hollow on top of a subsurface O (H_O), the bridge between two surface O (B_O), and the hollow on top of a subsurface Ce (H_{Ce}). The following defective surfaces were also considered: a Cu adatom on a defective ceria surface (denoted as $Cu@O^v$), a Cu adatom substituting for a Ce ion ($Cu@Ce^v$), and a Cu adatom substituting for a Ce ion with an O vacancy nearby ($Cu@Ce^vO^v$). All of them were modeled with the same supercell described above. The possible effect on the energetics of surface dipoles formed by the adsorbates were checked by adding a compensating electric field and the results were shown to be affected by less than 0.01 eV.

Structural relaxations according to the Hellmann–Feynman forces were performed for all the systems described above. During the relaxation the lowermost O–Ce–O layers were fixed to the equilibrium positions of the surface supercell described above. The atomic positions were relaxed until the force acting on each atom was smaller than 0.01 eV/Å. Before relaxation, the crystal structure of the adsorbate was perturbed so as to allow a symmetry-unconstrained structural optimization.

B. Surface thermodynamics

The effect of temperature and pressure on the relative stability of the Cu/CeO_2 surface structures was studied by employing the formalism of *ab initio* thermodynamics. In this framework, the free energy of formation of a general Cu/CeO_x surface structure, $\Delta G(T, p)$ (defined below), is assumed to depend on temperature and pressure only via the oxygen chemical potential $\mu_O(T, p)$

$$\mu_O(T, p) = \mu_O(T, p^0) + \frac{1}{2}kT\ln\left(\frac{p}{p^0}\right). \quad (1)$$

The latter describes the thermodynamic reservoir of the O_2 environment that is in contact with the surface under analysis. In particular, we will calculate free energy differences as a function of $\Delta\mu_O(T, p) = \mu_O(T, p) - \mu_O(T = 0\,\mathrm{K}, p^0)$, i.e., changes of oxygen chemical potential with respect to a zero reference state, which we set to the total energy of the O atom in an isolated molecule at $T = 0$ K, $\mu_O(T = 0\,\mathrm{K}, p^0) = 1/2E_{O_2} = 0$. The calculated value of the latter has been compensated for the known over binding of the molecular O_2 predicted by the current approximations in the exchange and correlation functionals. Vibrational and rotational entropic contributions to $\mu_O(T, p)$ are included by means of thermodynamic tables, as described in Ref. 43. In these assumptions, and neglecting entropic contributions of the solids involved, the free energy of formation can be calculated as

$$\Delta G(T, p) = E_{Cu/CeO_x} - E_{CeO_2} + N_O^v\mu_O(T, p) + N_{Ce}^v[e_{CeO_2}^{bulk} - 2\mu_O(T, p)] - \mu_{Cu}, \quad (2)$$

in terms of the total energies of the supercell modeling the specific Cu–CeO_2 surface structure (E_{Cu/CeO_x}) and the one modeling the corresponding stoichiometric surface (E_{CeO_2}). The energy cost for the formation of the surface defects (O or Ce vacancies) that are possibly present into the structure under analysis is also included by considering the number of such defects in the supercell (N_O^v and N_{Ce}^v, respectively) via the chemical potential of O ($\mu_O(T, p)$) and of bulk CeO_2 ($e_{CeO_2}^{bulk}$). Finally, the calculated formation energies $\Delta G^f(T, p)$ are referred to the chemical potential of Cu, μ_{Cu}, which we set as the total energy per atom of bulk Cu-fcc crystal. Note that the Ce_2O_3 phase becomes more stable than the CeO_2 for very low values of the chemical potential $\Delta\mu_O(T, p) < -4.11$, (Ref. 55), which should be considered as a lower boundary in our thermodynamic analysis.

In order to facilitate the comparison with the available literature, we will also report the adsorption energy (E_{ads}) calculated in terms of the following total energies of individual supercells: $E_{ads} = E_{Cu/CeO_x} - (E_{CeO_x} + E_{Cu})$, where E_{Cu/CeO_x} and is the total energy of the complete system (i.e., Cu adatom interacting with the surface), E_{CeO_x} is the total energy of the corresponding ceria surface (stoichiometric or reduced) and E_{Cu} is the total energy of a copper atom isolated in vacuum.

C. The Cu(111)/CeO_2 interface

The coherent $Cu(111)/CeO_2(111)$ interface was modeled with a hexagonal supercell comprising (2×2) surface units for the CeO_2 and (3×3) surface units for the Cu slab. This choice was determined by the ratio between the equilibrium lattice parameters of ceria and copper crystals (5.41 and 3.63 Å, respectively[32,56–59]), which is very close to 2:3. This is indeed supported by LEED pattern for the $Cu(111)/CeO_2(111)$ interface displaying a 1.5×1.5 periodicity.[20,60,61]

The computational supercell consisted of four Cu layers and three CeO_2 trilayers. We note, however, that the results reported in the following are independent on whether three or two CeO_2 trilayers are included in the supercell. In fact, the determination of the minimum-energy configuration with respect to relative shifts of the metal and oxide in the plane of the interface was performed by means of a thinner

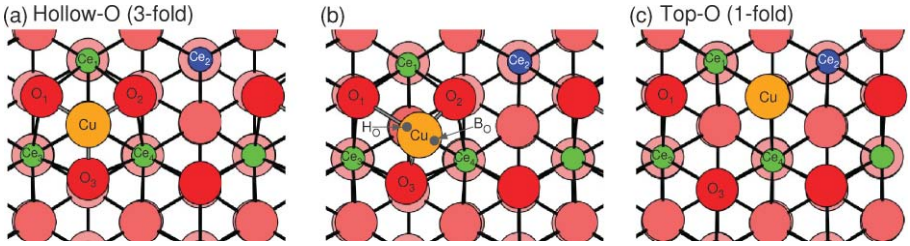

FIG. 2. Top view of the most stable adsorption configurations for a Cu adatom on the stoichiometric $CeO_2(111)$ surface.

supercell involving two instead of three CeO_2 trilayers. This was done so as to enforce structural equivalence of the two interfaces resulting from periodic boundaries for any value of the relative shift. The equilibrium configuration of the interface turned out to have enough symmetry to be described also by the thicker supercell, still preserving the structural equivalence of the periodic interface replicas. All atoms were allowed to relax except the two inner layers of copper atoms and the inner ceria trilayer that were fixed to their initial bulk-like coordinates. The atomic positions were relaxed until the force acting on each atom was less than 0.01 eV/Å.

III. RESULTS

A. Cu adatom on the stoichiometric CeO_2 surface

Our calculations predict the existence of three stable adsorption geometries for a Cu adatom on the stoichiometric (111) ceria surface, the most stable being the hollow H_O site displayed in Fig. 2(a). The relevant results for the adsorption energetics and atomistic structure are summarized in Table I. The Cu atom binds to the ceria surface with an adsorption energy of −3.03 eV, a large value when compared to the corresponding one calculated for other metal adsorbates on the same surface: −1.18 eV for Au,[42,44] −1.55 for Ag,[47] −1.71 eV for Pd,[62] and −2.62 for Pt.[63] The strong metal-oxide interaction is reflected in the radial displacement of its three nearest neighbors O atoms toward the adsorbate, resulting in a Cu–O bondlength of 2.03 Å and in three next-nearest neighbor Cu–Ce distances of 2.89 Å. This lowest energy structure is good agreement with recent calculations.[47,48] Some differences with these works concern the electronic structure predicted for the Cu/CeO_2 system, that will be discussed in the following.

TABLE I. Adsorption energy (E_{ads}) and free energy of formation (ΔG^0, calculated at $\Delta\mu = 0$); Spin magnetic moments of the Cu and Ce atoms (μ_{Cu} and μ_{Ce}); Elevation of the Cu adatom over the O atoms of the clean surface (d_z); Shortest Cu–O and Cu–Ce bondlengths (d) obtained from GGA+U (U = 4.5 eV) calculations. Corresponding results obtained by setting the value of U to 2.5 eV or the lattice parameter to the experimental value are indicated in squared brackets and parenthesis, respectively.

	H_O	B_O-H_O	T_O
E_{ads} [eV]	−3.03	−2.91	−2.15
	$[-2.49]_U$	$[-2.47]_U$	$[-1.67]_U$
	$(-2.86)_{a_0}$	$(-2.73)_{a_0}$	$(-2.00)_{a_0}$
ΔG^0 [eV]	0.47	0.58	1.33
μ_{Cu} [μ_B]	0.00	0.00	0.01
	[0.00]	[0.00]	[0.05]
	(0.00)	(0.00)	(0.01)
μ_{Ce} [μ_B]	1.01 × 1	1.01 × 1	1.01 × 1
	0.00 × 3	0.00 × 3	0.00 × 3
	[0.96]	[0.96 × 1]	[0.80 × 1]
	(1.00)	(1.00 × 1]	(1.00 × 1)
d_z(Cu)[Å]	0.91	0.99	2.05
d(Cu–O)[Å]	2.03 × 3	1.91 × 2	1.18 × 1
		2.71 × 1	
d(Cu–Ce)[Å]	2.89 × 3	2.72 × 1	3.68 × 2
		3.13 × 2	3.77 × 1

The copper–ceria interaction is accompanied by a charge transfer from the metal to the supporting oxide, as clearly evidenced by the bonding charge analysis displayed in Fig. 3, which reports the spatial distribution of the charge density difference (panel b) and the corresponding integrated values on planes parallel to the surface (panel a). This results in (i) a positively charged Cu adatom, which, on the basis of the following charge analysis can be identified as Cu^+, and (ii) in the localization of one electron on one Ce ion, which reduces to Ce^{3+}. The full electron localization is strongly coupled to a specific distortion of the crystal lattice, increasing the Ce–O bondlengths around the reduced Ce ions, as in the case of oxygen vacancies.[46] Quite similarly, here also the excess electron resulting from the metal adsorbate can localize on different cations, either close or far from the Cu atom (correspondingly Ce_1 and Ce_2 in Fig. 2), the latter configuration being lower in energy. We note that previous calculations[47,48] reported a distribution of the charge transferred to the oxide more delocalized over the three surface Ce ions. This is likely at the basis of the smaller binding energies reported in those studies (−2.79 and −2.68 eV) as compared to the present work (−3.03 eV).

The total and atom-projected densities of electronic states (DOS and PDOS, respectively) displayed in Fig. 3(c) further support the full reduction of one Ce ion of the oxide surface. This analysis shows the appearance of the filled f state for the Ce_2 ion, yielding the calculated magnetic moment of $1.01\mu_B$ (see Table I), while all the other Ce ions in the supercell remain unreduced. This feature in the electronic structure is in the same energy range of the metal-oxide bonding arising between the Cu-d and the O-p states. The angular-momentum decomposition of the PDOS for the Cu adsorbate [Fig. 2(c)] shows that all the d states are filled, forming two bands just above the top of the O-2p valence band of the oxide, while the s states are empty thus supporting the interpretation of the Cu adatom on the stoichiometric CeO_2 surface as an ionic Cu^+ adspecies.

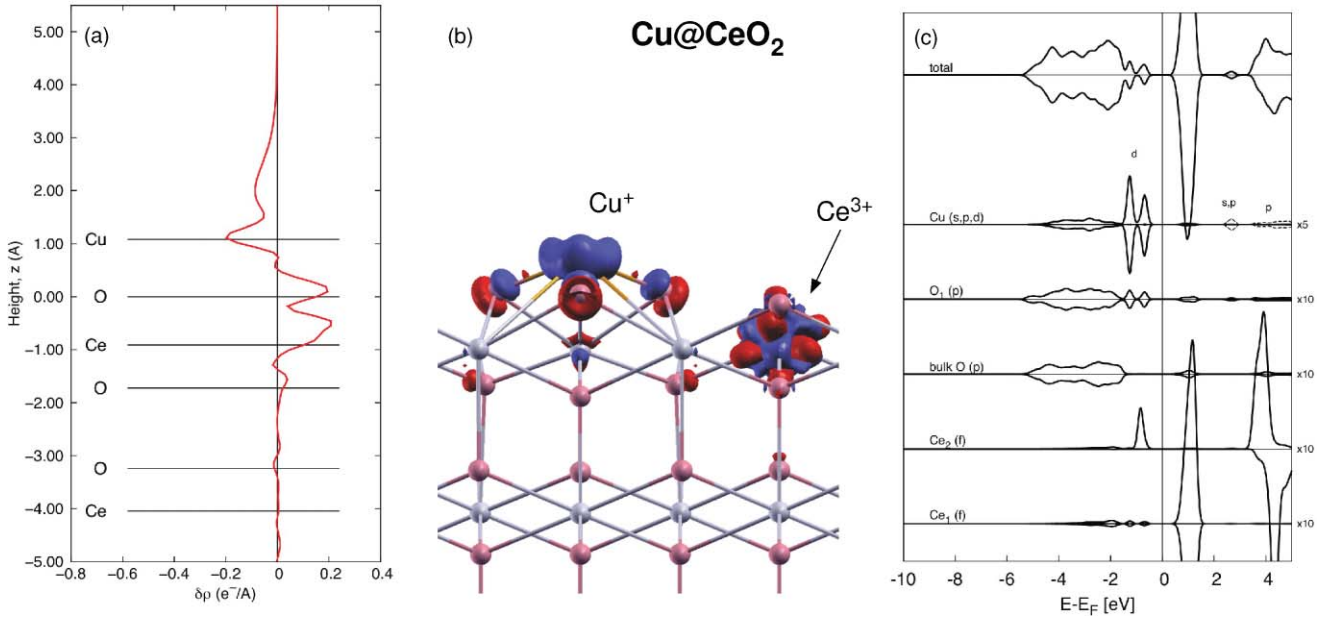

FIG. 3. Bonding charge and DOS for a Cu adatom supported by the stoichiometric (111) CeO_2 surface in the lowest energy H_O site. (a) Bonding charge integrated in planes perpendicular to the surface and plotted as a function of the height from the surface. (b) Bonding charge plotted at the value of 0.07 $e/Å^3$ (Electron accumulation and depletion are represented by dark (red) and light (blue) areas, respectively). (c) Total DOS and atom-resolved projected DOS analysis. Energies are referred to the Fermi level (vertical solid line).

The lowest energy H_O solution, which is very symmetric and involves the bonding of the Cu adatom with three surface O atoms is almost degenerate with the one shown in Fig. 2(b), which is only 0.12 eV higher in energy (Table II). In this equilibrium H_O–B_O configuration, the Cu adatom is right in between the ideal hollow and bridge surface sites, it is bound to only two O atoms thus yielding two shorter (1.91 Å) and one longer (2.71 Å) Cu–O bondlengths. As such, it is separated from the H_O configuration by an energy barrier required to displace the O_1 and the Cu atoms to form the third Cu–O bond. Besides this structural difference, the electronic structure of the two adsorption sites is the same, both in terms of charge transfer and of full reduction of the Ce_2 ion, as demonstrated for instance by the spin magnetic moment of the Ce atoms (Table I). Also in this case there are several stable Ce sites available for the localization of the excess electron, the lowest energy being again the Ce_2 site, which in the present supercell is the farthest from the adsorbate. We could also stabilize the other configurations with a reduced cerium on the Ce_1 and Ce_3 sites [see Fig. 2(b)], which were 0.39 and 0.19 eV higher in energy, respectively.

TABLE II. Energy of adsorption (E_{ads}) and free energy of formation (ΔG°, calculated at $\Delta\mu = 0$) for a Cu atom at point defects of the CeO_2(111) surface; spin magnetic moments of the Cu and Ce atoms (μ_{Cu} and μ_{Ce}); elevation of the Cu adatom over the O atoms of the clean surface (d_z); Shortest Cu–O and Cu–Ce bondlengths (d).

	Cu@O^v	Cu@Ce^v	Cu@CevO^v
E_{ads} [eV]	−1.58	–	–
ΔG° [eV]	4.39	−0.44	−0.16
μ_{Cu} [μ_B]	0.01	0.00	0.50
μ_{Ce} [μ_B]	0.98 × 1	0.00 × 4	0.00 × 4
	0.03 × 3		
d_z(Cu) [Å]	1.22	−1.55	−1.49
d(Cu–O) [Å]	3.37	1.84 × 3	1.95 × 3
	3.56 3.57	1.87 × 1	1.97 × 1
d(Cu–Ce) [Å]	3.09 × 2	3.22 × 4	3.22 × 3
	3.20 × 1		3.12 × 1

The adsorption configuration on top of a surface O atom T_O was also found to be stable ($E_{ads} = -2.15$ eV), but considerable higher in energy (+0.86 eV) than the lowest energy H_O one. This T_O binding geometry displays the same charge transfer and electron localization effects described above for the lowest energy cases and leading to the formation of a Cu^+ surface species and the reduction of the ceria support, which are therefore general conclusions independent on the adsorption site. The structural optimizations started from the Cu adsorbate on the H_{Ce} and B_{Ce} sites relaxed into the same H_O–B_O equilibrium configuration described above.

It is important to prove that these results are not dependent on the actual value of the parameter U used in the calculations (provided it is large enough to destabilize fractional occupancy of the Ce-f states and drive electron localization). We report in Table I the energetics and spin magnetic moments calculated with a value of U = 2.5 eV (squared brackets) and resulting from a single-point self-consistent calculation in which the lattice parameter was set equal to the experimental one, 5.41 Å (values in parentheses). As noted for closely related systems, this analysis shows once again that the actual values of the energetics depend on the value of U (adsorption energies changes by 0.5 eV when U span the 2.5–4.5 interval), but the relative differences (and hence the hierarchy of the adsorption sites) are almost unchanged. Most importantly, the charge transfer from the Cu adatom to the ceria support and the reduction of ceria (resulting from the full localization of one electron on one surface Ce ion) is displayed by all these calculations (i.e., unaffected by variations

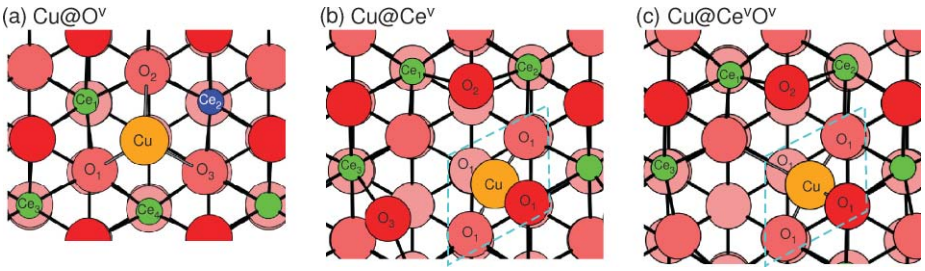

FIG. 4. Adsorption geometry for a Cu adatom on/in defective $CeO_2(111)$ surfaces: (a) above an O-vacancy (Cu@O^v), (b) substituting for a Ce ion in a solid solution (Cu@Ce^v), and (c) substituting for a Ce ion in the presence of an O vacancy nearby (Cu@Ce^{v}O^v). The dashed lines mark the characteristic CuO_4 squared planar moiety in the solid solutions.

of the U and ceria lattice parameters), and can therefore be considered as a robust prediction of the simulations.

B. Cu adatom on the reduced CeO_{2-x} surface

The lowest energy configuration for a Cu atom adsorbed on top of an O vacancy of a reduced CeO_{2-x} surface is displayed in Fig. 4(a) and the main energetics and structural parameters are summarized in Table II. The calculated adsorption energy (E_{ads}) is −1.58 eV, higher by 1.45 eV than the one on the stoichiometric surface. The weaker bonding of the adsorbate on the defective as compared to the stoichiometric ceria (111) surface is distinctive of Cu adsorbates.

Also in this case, the analysis of the bonding-charge displayed in Fig. 5 reveals a marked charge reorganization and transfer across the metal–oxide interface, but in the opposite direction with respect to the Cu adsorption on the stoichiometric surface. Starting from a reduced surface with an O vacancy and two reduced Ce^{3+} ions, the presence of a Cu adsorbate drives charge from the surface to the Cu adsorbate, which therefore becomes a negatively charged $Cu^{\delta-}$ species, in analogy to the corresponding case of Au.[42–44] This is clearly shown by the plane integrated bonding charge [Fig. 5(a)], showing charge depletion in the Ce layer and accumulation between the Cu and the O vacancy. The DOS analysis [Fig. 5(b)] provides evidence that this charge transfer leads to the presence of only one reduced Ce^{3+} ion and a $Cu^{\delta-}$ adsorbate. The angular momentum resolved PDOS shows that the Cu-*d* states are all filled and form a sharp gap state right above the O-2*p* valence band of ceria. In addition, the same analysis shows also the filling of the Cu-*s* and the partial occupancy of the Cu-*p* states. Of the four surface Ce ions, only one (Ce_2) is fully reduced to Ce^{3+}, with a spin magnetic moment of 0.98 μ_B, while the other three are not spin polarized (Table II). This is different than the result of Yang *et al.* reporting that about 1.5 electrons are equally distributed between the three Ce ions neighboring the Cu adsorbate.[48] In the DFT+U scheme, such fractional occupancies are subject to an energy penalty, which is probably at the origin of the smaller value of adsorption energies reported in that study (−1.46 eV).

The broken symmetry of the electron localization on the Ce ions is reflected into the equilibrium adsorption geometry of the Cu adatom, reporting two short (3.09 Å) and one long

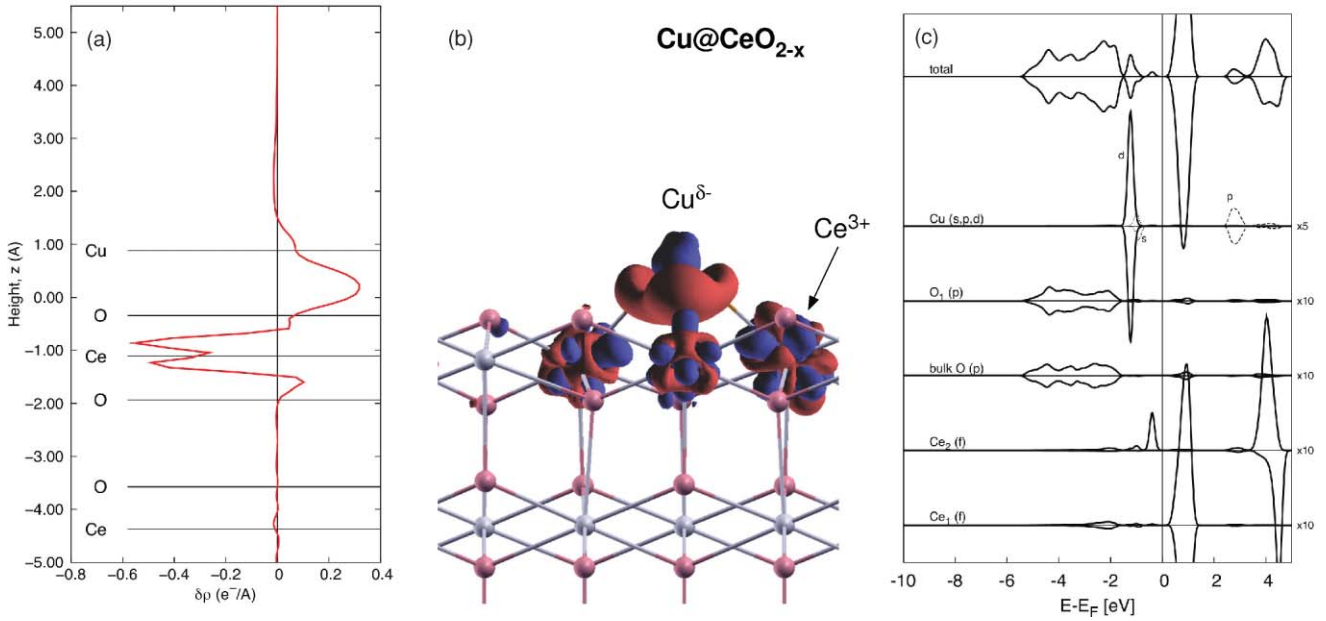

FIG. 5. Bonding charge ($\delta\rho$, panels a and b) and density of electronic states (DOS, PDOS, panel c) for a Cu atom adsorbed on an O vacancy of a reduced (111) CeO_{2-x} surface.

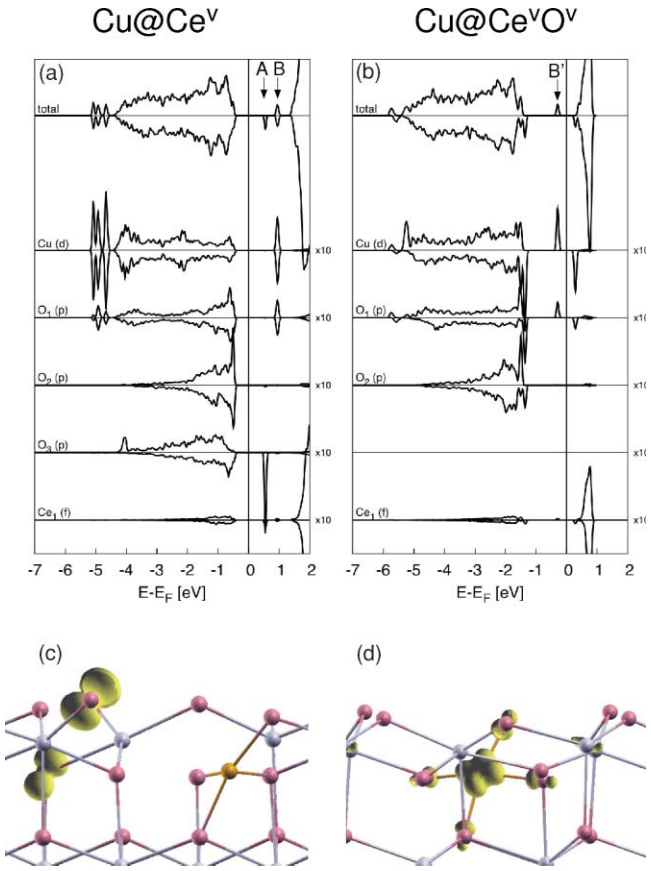

FIG. 6. Density of electronic states for (a) the Cu@Ce^v and (b) the Cu@Ce^{v}O^v structures and corresponding electron spin densities [(c) and (d)].

(3.20 Å) Cu–Ce bondlengths, the latter being between the adsorbate and the reduced Ce^{3+} ion.

C. Cu/CeO_2 solid solutions

The solid solution resulting when a Cu atom substitutes for a Ce ion in the second layer of the CeO_2(111) surface presents a characteristic local reconstruction around the Cu site, leading to a squared planar CuO_4 unit [see dashed lines in Fig. 4(b)]. This local configuration arises from a considerable surface rearrangement, in which the Cu ion displaces from the second atomic layer to the third one. In the final equilibrium configuration, the Cu atom lies 1.55 Å below the outermost surface O atoms. The four O atoms (O_1 in Fig. 4) of the CuO_4 unit and neighboring the Cu ion are located in the first (one neighbor), third (two neighbors), and fourth (one neighbor) atomic layer, with bondlengths of 1.84–1.87 Å (see Table II). In addition, two surface O atoms (O_2 and O_3 in Fig. 4) displace away from the Cu site by as much as 0.89 Å, resulting in strongly undercoordinated surface O atoms. It is not surprising that these O atoms are very labile and can easily lead to O vacancy formation, as discussed in the thermodynamics analysis presented in the following section.

The surface structure denoted by Cu@Ce^{v}O^v [Fig. 4(c)] is obtained by removing one of these undercoordinated surface O atoms (O_3, which is the least bound to the surface). The CuO_4 unit is very stable upon vacancy formation at the nearby surface O site, the main change being an increase in the Cu–O bondlengths, from 1.84–1.87 to 1.95–1.97 Å (Table II). We note that this squared-planar structure is analogue to the one formed by other transition metals substituting for Ce in ceria surfaces, such as Au[48,49,64] or Pd.[65]

Both these solid solutions, Cu@Ce^v and Ce@Ce^{v}O^v, turn out to be insulating. Contrary to the cases of Cu adatoms supported by stoichiometric and reduced ceria, the binding of Cu atoms at Ce vacancies do not drive the reduction of Ce ions nearby. This is clearly shown in the electronic DOS and PDOS displayed in Fig. 6. Electron gap states are present in both solid solutions, but these are not related to the Ce f states, which form the sharp band typical of stoichiometric CeO_2. In Cu@Ce^v, there are two unoccupied gap states [see arrows in Fig. 6(a)]. The lowest energy one (A) determines the spin polarization of the Cu@Ce^v structure (1.00 μ_B) and results from the dangling bond of the undercoordinated surface O_3 ion. The spin density [Fig. 6(c)] shows that this state is localized mostly on the O_3 surface atom (71%) and on the O atom directly underneath (29%). The higher energy gap state (B) results instead from the Cu(d)–O(p) hybridization in the CuO_4 unit leading to the oxidation of the Cu atom (the calculated Lowdin charge population of the Cu-d orbitals is 0.93).

The excess electrons made available upon vacancy formation on the Cu@Ce^v structure by removing altogether the unsaturated O_3 atoms (and hence the unoccupied state A described above) allow for the occupation of the spin up component of the Cu–O state [B′, Fig. 6(b)]. The resulting electronic structure [see Fig. 6(b)] is still insulating and spin-polarized (1.00 μ_B), but the spin density is now strongly localized on the CuO_4 moiety [Fig. 6(d)].

D. Thermodynamics of adsorption

We report in Fig. 7 the free energy of adsorption ΔG^a as a function of changes in the chemical potential of O with respect to the reference $\Delta\mu_O$. This thermodynamic analysis shows that Cu adsorption on the stoichiometric surface is more stable than on O vacancies at all temperatures and pressures relevant for catalytic applications. This, therefore, suggests that O vacancies do not act as anchoring sites for the nucleation of Cu nanoparticles on ceria surfaces. This is at variance with other transition-metals supported on CeO_2 (111), most notable Au, where reducing conditions strongly favor the adsorption of adatoms on surface O vacancies.[43,64]

In oxidative environments, the two solid solutions described above (Cu@Ce^v and Cu@Ce^{v}O^v) become thermodynamically more stable than the supported adatoms. At the reference conditions traditionally used in most computational studies (the energy of an O atom in an O_2 molecule at $T = 0$), the Cu@Ce^v system is more stable than the Cu@Ce^{v}O^v, but their relative stability is quickly modified by increasing T and p, and is actually reversed already at ambient conditions. Quite importantly the slopes of the thermodynamic boundaries governing the relative stability of the two structures are such that, in chemical conditions where solid solutions are stable, the energy difference between them is always smaller than 0.3 eV. In this perspective, the role of the substitutional

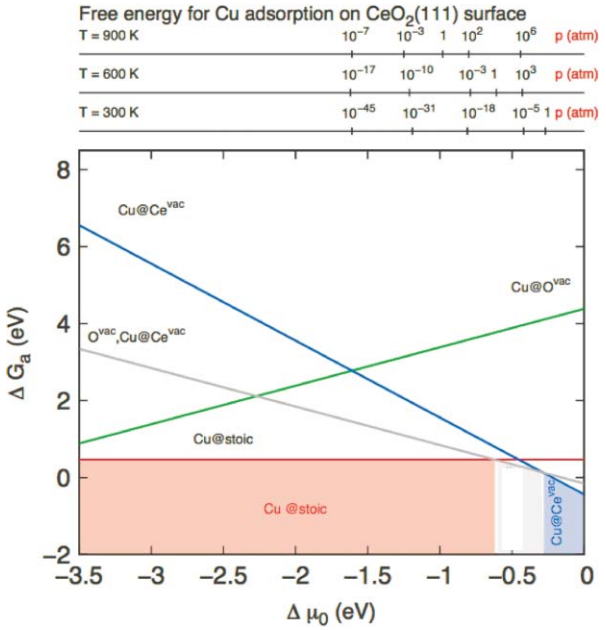

FIG. 7. Free energy for Cu adsorption (ΔG) on the stoichiometric and defective $CeO_2(111)$ surface as a function of changes in the chemical potential ($\Delta\mu_O$).

Cu ion is to stabilize surface structures capable for an easy and reversible O release at thermodynamic conditions relevant for real catalysis. Quite importantly, the reversible O release is not accompanied by ceria reduction via the $Ce^{4+} \leftrightarrow Ce^{3+}$ dynamics.

E. Cu(111)/CeO_2(111) interface

The analysis of the Cu(111)/CeO_2(111) interface (Fig. 8) presents a larger number of structural degrees of freedom and has been performed in steps. First we determined the minimum-energy relative position of the ceria and Cu slabs by considering their rigid translation in the interface plane at fixed distance of the interfacial Cu–O planes (3.0 Å). To this end, we performed a set of self-consistent calculations at the DFT level on a 2D grid of relative displacements separated by approximately 0.05 Å in the x and y directions. Note that the symmetry of the system at the interface allows for reducing the analysis to the irreducible triangle highlighted in the inset of Fig. 8(c) and having periodicity of 0.3 Å. The periodicity was verified numerically by considering several greater shifts in the whole supercell.

The global minimum-energy configuration resulting from the 2D total-energy landscape was then used to determine the equilibrium Cu–O distance (Δz) at the interface, as shown in Fig. 8(b). This analysis predicts a separation between the ceria and copper slabs of 2.1 Å. Finally the total energy as a function of the in-plane displacement of one slab with respect to the other was explored again for this value of optimal Δz. The resulting DFT+U 2D energy landscape is displayed in the inset of Fig. 8(c), where the darkest areas map the configuration with the minimum energy, while the lightest color indicates configurations 0.24 eV higher in energy. Note that plain DFT calculations would predict the same minimum-energy interface configuration but, as in the other cases involving electron localization, a completely different interface electronic structure.

The atomic coordinates of the minimum-energy interface configuration resulting from the rigid-block analysis described above were then optimized according to the Hellmann–Feynmann forces. The resulting equilibrium configuration is shown in Fig. 8(c) and displays two specific Cu–O interface local structures. In the first one, one of the interface O atoms of the oxide is atop of a Cu atom (at 1.89 Å, see Table III). In the second one, which occurs in three equivalent but rotated variants in the same supercell, the O atom is bridging between two Cu atoms (at 2.04 Å). There are two remaining interfacial Cu atoms in the supercell that are not directly bound to the oxide, one on top of a second-layer Ce atom (at 3.12 Å) and one on top of a third-layer O atom. Note that the two interfaces resulting from periodic boundary conditions are equivalent, so Table III reports values for only one interface.

The same charge transfer from the metal to the stoichiometric surface reported for the case of Cu adatoms takes place also at the metal–oxide interface, but the effect is magnified due to the larger contact area. It turns out that four electrons are transferred to the f states of the four Ce_1 ions in the supercell, resulting in full reduction of the first ceria trilayer in contact with the metal. This is shown by the bonding charge and atom-projected DOS shown in Fig. 9. The interfacial Cu_1 and O_1 atoms display charge reorganization leading to charge accumulation in the interface region and directional localization between the Cu and O interfacial atoms. The formation of Cu–O bonds is further supported by the shortening of the Cu–O bond lengths by 0.23–0.45 Å with respect to their position in the respective free-surface coordinates. In particular, the equilibrium Cu–O interfacial bond lengths 1.89 and 2.04 Å are compatible with those of bulk Cu_2O (1.84 Å Ref. 66), thus showing the tendency to locally form copper oxide at the metal–oxide interface. In addition, the charge transfer leads to the reduction to Ce^{3+} of all the Ce ions closest to the metal (Ce_1), as clearly shown by the occupied f-state in the DOS and by their spin magnetic moment of 1.00 μ_B (Table III). The analysis of the DOS allows also to conclude that the effect of the interface on the electronic structure is very short range, since the second trilayer is already bulklike.

In conclusion, our calculations predict the oxidation of the interfacial Cu atoms in contact with ceria, and the full reduction of the first ceria trilayer, which contains exclusively Ce^{3+} ions. We finally note that a plain DFT calculation would predict a completely different description of this interface bonding, displaying charge localization between the Cu and Ce ions instead of on the Ce-f states. This electron localization versus delocalization issue of excess electrons on the Ce f states described by DFT and DFT+U approaches has been discussed extensively in the literature in the context of point defects. The case of this interface shows once again the importance of going beyond DFT for a qualitatively correct description of bonding and charge density in ceria-based materials.

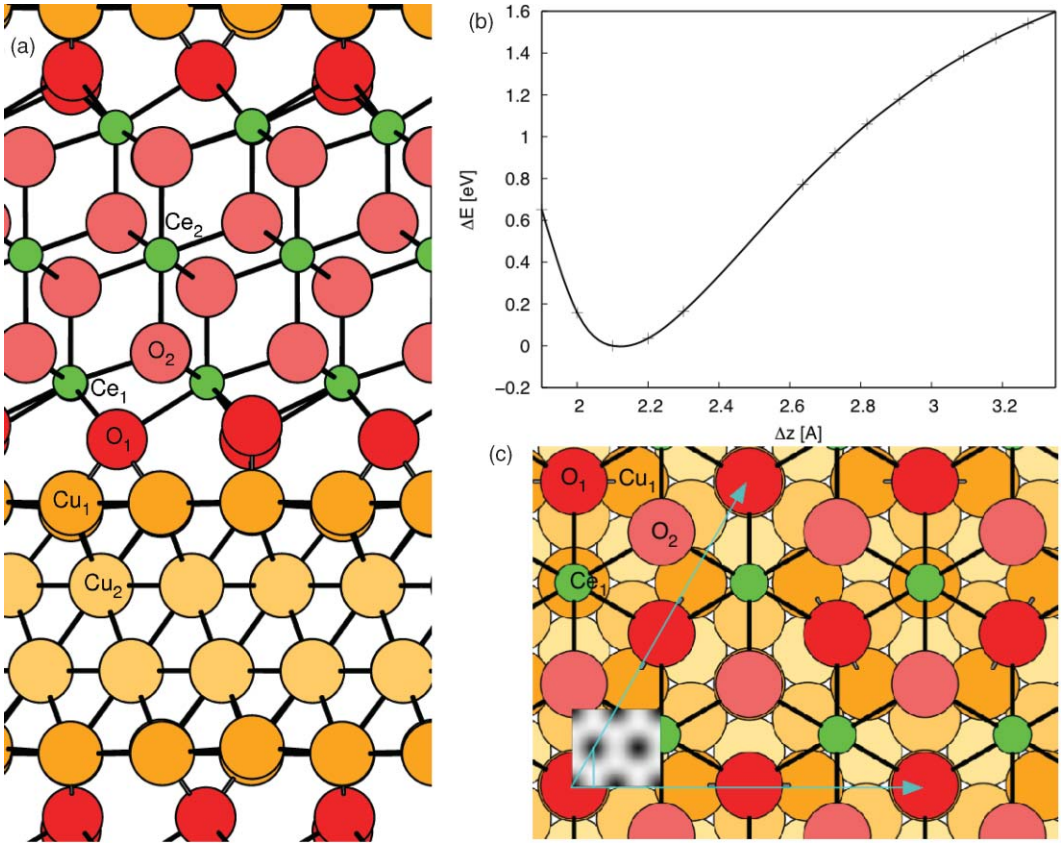

FIG. 8. Side (a) and top (c) view of the supercell slab used to describe the $CeO_2(111)/Cu(111)$ interface, displaying the lowest-energy equilibrium structure. (b) Total energy vs interfacial distance (Δz). The inset in panel (c) display the 2D total-energy landscape for the relative displacement of the metal and oxide supercells in the interface plane. Black represents the minimum energy configurations, while the lightest regions are 0.24 eV higher in energy.

IV. DISCUSSION

Even without taking into account the energy to form O vacancies on the surface, these results demonstrate a strong selectivity for the adsorption of Cu adatoms on stoichiometric regions of the surface rather than on O vacancies. The binding of Cu adatoms on $CeO_{(2-x)}(111)$ is 1.45 eV weaker than on $CeO_2(111)$. The thermodynamic analysis shows that this relative stability holds for a wide range of pressure and temperatures, including those relevant for most catalytic applications of Cu/ceria systems. In addition, the combined process of defect formation (calculated value 2.15 eV) and Cu adsorption (−1.58 eV) is overall endothermic by 0.6 eV. In the context of metal adatoms supported by ceria surfaces, these results have important implications on the surface mechanisms active on ceria-based catalysts.

TABLE III. Spin magnetic moments of the Cu and Ce atoms (μ_{Cu} and μ_{Ce}) and shortest Cu–O and Cu–Ce bondlengths calculated in the $Cu(111)/CeO_2$ interface. Atoms are labeled as in Fig. 8.

μ_{Cu_1} [μ_B]	0.00 × 4
μ_{Ce_1} [μ_B]	0.98 × 4
μ_{Ce_2} [μ_B]	0.00 × 4
d_z(Cu) [Å]	1.58–1.89
d(Cu_1–O_1) [Å]	1.89 × 1
	2.04 × 6
d(Cu_1–Ce_2) [Å]	3.12 × 1
	3.28 × 6

Several studies demonstrated that Au adatoms on the same ceria surface display a strong driving force for binding to surface defects [more than 1.1 eV (Refs. 42, 44, and 67)] relatively to the stoichiometric surface. The defects constitute therefore nucleation and anchoring sites for larger metal clusters.[68] In that case, the overall process of vacancy formation and Au adsorption is slightly exothermic. Similar preferential adatom adsorption on O vacancies of ceria was also reported for Pd and Pt.[62,63] Among the metal adsorbates addressed to date, Cu is the only one which is predicted to form Cu^+ species that are stable also in the presence of O vacancies, even in reducing conditions and we ascribe this.

Therefore these results predict that Cu nanoparticles will not nucleate on surface O vacancies but will rather be supported by stoichiometric ceria surfaces. The situation seems to be similar to the case of TiO_2/metal systems,[69] where gold nanoparticles nucleate on defects—steps or vacancies, while Cu is reported to grow both on terraces and steps, due to the larger adsorption energy at stoichiometric surface (−1.76 eV) than on O vacancies (−0.94 eV).

Copper nanoparticles are then likely to grow exposing the (111) planes to the most stable $CeO_2(111)$ terraces, as reported in Ref. 20 for conventional copper-loaded ceria nanopowder catalyst. Our model $Cu(111)/CeO_2(111)$ interface would then be representative of the inner contact area between ceria and the Cu nanoparticle, sufficiently

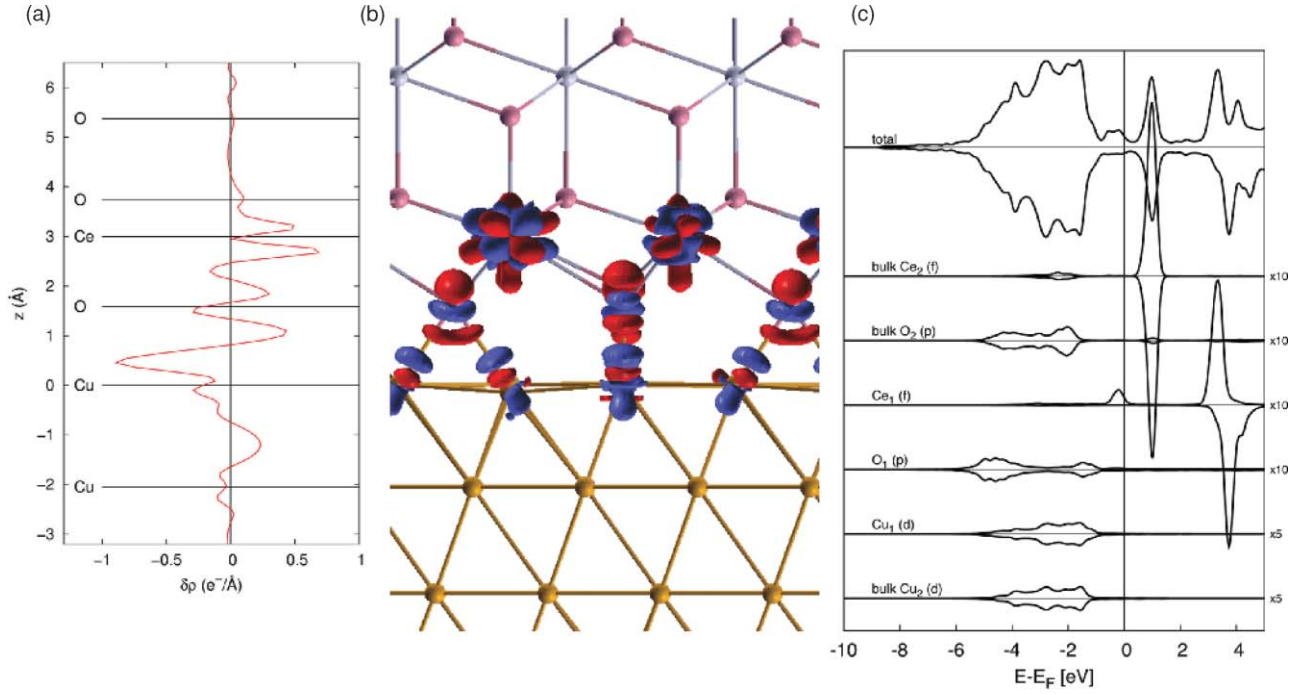

FIG. 9. Bonding charge ($\delta\rho$, panels a and b) and density of electronic states [DOS, PDOS, panel (c)] for the Cu(111)/CeO_2 interface.

away from the outer edge of the cluster. Based on our results, we then propose that the Cu particle fully reduces the first ceria trilayer directly underneath, leading to the presence of a "shadow" of reduced Ce^{3+} ions that extends up to the perimeter of the metal/oxide interface. The reduction of ceria in presence of copper was indeed reported in Ref. 20 by means of X-ray and synchrotron radiation photoemission spectroscopies (XPS and SRPES) and resonant photoelectron spectroscopy both in conventional and inverse model catalysts. Quite importantly, both these systems showed also higher activity toward CO oxidation, therefore our results concerning the electronic and structural characterization of the metal–ceria interface are the starting point for understanding the improved catalytic performance of these systems.

This is related to the possible reaction mechanism and stability of the supported metal particles. In our previous study on the Au/ceria system,[44] we showed that the Au^+ surface species resulting from the metal–oxide interaction are very active toward CO adsorption and oxidation. However, the participation of lattice O into the reaction involves the formation of O vacancies that, in the case of the ceria/Au system, are shown to attract the Au adatom and turn it into negatively charged $Au^{\delta-}$ surface species. In the case of Au, the diffusion of the active species from the stoichiometric surface into O vacancies (driven by the largest adsorption energy on the vacancy site) determines the deactivation of the catalyst. The same mechanism is likely to be active until the cluster size is large enough so that its cohesion would prevent the attraction of the interfacial Au atoms into the vacancies. The supported Cu^+ species are instead stable toward diffusion into the O vacancies formed during CO oxidation and will not be deactivated during a similar reaction mechanism.

V. CONCLUSIONS

We have provided a comprehensive computational study based on the DFT+U method of the electronic and structural properties of Cu/Ceria interfaces, modeling surface solid solutions and the contact at the smallest Cu supported clusters (Cu adatoms) as well as at large metal particles. Ce^{3+} species are always present underneath Cu particles supported by stoichiometric and reduced ceria (111) surfaces, resulting from charge transfer across the metal/oxide interface. The result is proved to be robust on the computational parameters. The calculated surface thermodynamics shows that adsorption on surface O vacancies is disfavored with respect to binding on stoichiometric regions of the surface even in extremely reducing chemical environments. O vacancies are therefore not relevant for the thermodynamic stability and nucleation of larger metal Cu nanoparticles. In oxidizing conditions, Cu/CeO_2 solid solutions, in which Cu atoms are dispersed as substitutional point defects, become more stable than supported adatoms. Ceria is not reduced by formation of these Cu point defects. The substitutional Cu ions stabilize characteristic CuO_4 units that allow for an easy and reversible O release in a range of thermodynamic conditions relevant for real catalysis. The O buffering of the Cu/CeO_2 solid solutions does not involve ceria reduction and electron localization–delocalization processes at Ce sites.

The interface between supported large nanoparticles and stoichiometric ceria was modeled with a coherent Cu(111)/CeO_2 interface. The calculations predict substantial charge transfer across the metal/oxide interface leading to the full reduction of the first ceria trilayer directly underneath the supported Cu particle. This "shadow" of Ce^{3+} ions below metal nanoparticles stems from the exceptional

ceria reducibility and can be related to the high catalytic reactivity of these systems, particularly for thin layers that are currently under analysis both with experimental and theoretical approaches.

ACKNOWLEDGMENTS

This work is a part of the research programs MSM 00216208 34 financed by the Ministry of Education of the Czech Republic, P204/10/1169 and 202/09/H041 financed by Czech Grant Agency and 103/406 financed by the Charles University Grant Agency. The Physics Department of Jan Evangelista Purkyně University in Ústí nad Labem is acknowledged for providing computer resources. The authors are grateful to F. Illas and M. M. Branda for fruitful discussions.

[1] N. Armaroli and V. Balzani, Angew. Chem., Int. Ed. **46**, 52 (2007).
[2] A. Trovarelli, *Catalysis by Ceria and Related Materials* (Imperial College, London, 2002).
[3] A. Trovarelli, Catal. Rev. -Sci. Eng. **38**, 439 (1996).
[4] W. Xiao, Q. Guo, and E. G. Wang, Chem. Phys. Lett. **368**, 527 (2003).
[5] W. Liu and M. Flytzani-Stephanopoulos, J. Catal. **153**, 304 (1995).
[6] W. Liu and M. Flytzani-Stephanopoulos, Chem. Eng. J. Biochem. Eng. J. **64**, 283 (1996).
[7] C. R. Jung, J. Han, S. W. Nam, T.-H. Lim, S.-A. Hong, and H.-I. Lee, Catal. Today **93**, 183 (2004).
[8] B. Wen and M. He, Appl. Catal., B **37**, 75 (2002).
[9] P. Bera, S. T. Aruna, K. C. Patil, and M. S. Hegde, J. Catal. **186**, 36 (1999).
[10] P. Djinovic, P. Batista, and A. Pintar, Appl. Catal., A **347**, 23 (2008).
[11] Y. Liu, T. Hayakawa, K. Suzuki, and S. Hamakawa, Catal. Commun. **2**, 195 (2001).
[12] J. Guzman, S. Carrettin, and A. Corma, J. Am. Chem. Soc. **127**, 3286 (2005).
[13] Q. Fu, H. Saltzburg, and M. Flytzani-Stephanopoulos, Science **301**, 935 (2003).
[14] J. A. Rodríguez, M. Pérez, J. Evans, G. Liu, and J. Hrbek, J. Chem. Phys. **122**, 241101 (2005).
[15] X. Wang, J. A. Rodríguez, J. C. Hanson, M. Pérez, and J. Evans, J. Chem. Phys. **123**, 211101 (2005).
[16] M. Škoda, M. Cabala, I. Matolínová, K. C. Prince, T. Skála, F. Šutara, K. Veltruská, and V. Matolín, J. Chem. Phys. **130**, 034703 (2009).
[17] L. Barrio, M. Estrella, G. Zhou, W. Wen, J. H. Henson, A. B. Hungria, A. Hornes, M. Fernandez-Garcia, A. Martínez-Arias, and J. A. Rodríguez, J. Phys. Chem. C **114**, 3580 (2010).
[18] E. Wahlström, N. Lopez, R. Schaub, P. Thostrup, A. Rønnau, C. Africh, E. Lægsgaard, J. K. Nørskov, and F. Besenbacher, Phys. Rev. Lett. **90**, 026101 (2003).
[19] D. Matthey, J. G. Wang, S. Wendt, J. Matthiesen, R. Schaub, E. Lægsgaard, B. Hammer, and F. Besenbacher, Science **315**, 1692 (2007).
[20] V. Matolín, L. Sedláček, I. Matolínová, F. Šutara, T. Skála, B. Šmíd, J. Libra, V. Nehasil, and K. C. Prince, J. Phys. Chem. C **112**, 3751 (2008).
[21] J. A. Rodríguez and J. Hrbek, Surf. Sci. **604**, 241 (2010).
[22] X. Wang, J. A. Rodríguez, J. C. Hanson, D. Gamarra, A. Martínez-Arias, and M. Fernández-García, J. Phys. Chem. B **110**, 428 (2006).
[23] J. A. Rodríguez, P. Liu, J. Hrbek, J. Evans, and M. Pérez, Angew. Chem. Int. Ed. **46**, 1329 (2007).
[24] S. Fabris, S. de Gironcoli, S. Baroni, G. Vicario, and G. Balducci, Phys. Rev. B **71**, 041102 (2005).
[25] S. Fabris, G. Vicario, G. Balducci, S. de Gironcoli, and S. Baroni, J. Phys. Chem. B **109**, 22860 (2005).
[26] M. Nolan, S. Grigoleit, D. C. Sayle, S. C. Parker, and G. W. Watson, Surf. Sci. **576**, 217 (2005).
[27] J. L. F. Da Silva, M. V. Ganduglia-Pirovano, J. Sauer, V. Bayer, and G. Kresse, Phys. Rev. B **75**, 045121 (2007).
[28] C. Loschen, J. Carrasco, K. M. Neyman, and F. Illas, Phys. Rev. B **75**, 035115 (2007).
[29] D. D. Koelling, A. M. Boring, and J. H. Wood, Solid State Commun. **47**, 227 (1983).
[30] G. A. Landrum, R. Dronskowski, R. Niewa, and F. J. DiSalvo, Chem. -Eur. J. **5**, 5515 (1999).
[31] N. V. Skorodumova, R. Ahuja, S. I. Simak, I. A. Abrikosov, B. Johansson, and B. I. Lundquist, Phys. Rev. B **64**, 115108 (2001).
[32] J. P. Perdew, J. A. Chevary, S. H. Vosko, K. A. Jackson, M. R. Pederson, D. J. Singh, and C. Fiolhais, Phys. Rev. B **46**, 6671 (1992).
[33] S. Hill and C. Catlow, J. Phys. Chem. Solids **54**, 411 (1993).
[34] N. V. Skorodumova, M. Baudin, and K. Hermansson, Phys. Rev. B **69**, 075401 (2004).
[35] Z. Yang, T. K. Woo, M. Baudin, and K. Hermansson, J. Chem. Phys. **120**, 7741 (2004).
[36] N. V. Skorodumova, S. I. Simak, B. I. Lundqvist, I. A. Abrikosov, and B. Johansson, Phys. Rev. Lett. **89**, 166601 (2002).
[37] S. Gennard, F. Corá, and C. R. A. Catlow, J. Phys. Chem. B **103**, 10158 (1999).
[38] J. C. Conesa, J. Phys. Chem. B **107**, 8840 (2003).
[39] M. Nolan and G. Watson, J. Phys. Chem. B **110**, 16600 (2006).
[40] M. Huang and S. Fabris, J. Phys. Chem. C **112**, 8643 (2008).
[41] M. Huang and S. Fabris, Phys. Rev. B **75**, 081404 (2007).
[42] C. Zhang, A. Michaelides, D. King, and S. J. Jenkins, J. Chem. Phys. **129**, 194708 (2008).
[43] C. Zhang, A. Michaelides, D. King, and S. J. Jenkis, J. Phys. Chem. C **113**, 6411 (2009).
[44] M. Farnesi Camellone and S. Fabris, J. Am. Chem. Soc. **131**, 10473 (2009).
[45] M. M. Branda, N. J. Castellani, R. Grau-Crespo, and F. Illas, J. Chem. Phys. **131**, 94702 (2009).
[46] M. V. Ganduglia-Pirovano, J. L. F. Da Silva, and J. Sauer, Phys. Rev. Lett. **102**, 026101 (2009).
[47] M. M. Branda, N. C. Henandez, J. F. Sanz, and F. Illas, J. Phys. Chem. C **114**, 1934 (2010).
[48] Z. Yang, B. He, Z. Lu, and K. Hermansson, J. Phys. Chem. C **114**, 4486 (2010).
[49] M. Nolan, V. S. Verdugo, and H. Metiu, Surf. Sci. **602**, 2734 (2008).
[50] J. P. Perdew, K. Burke, and M. Ernzherof, Phys. Rev. Lett. **77**, 3865 (1996).
[51] M. Cococcioni and S. de Gironcoli, Phys. Rev. B **71**, 035105 (2005).
[52] D. Vanderbilt, Phys. Rev. B **41**, 7892 (1990).
[53] L. Szabová, Master's thesis, Faculty of Mathematics and Physics, Charles University, Prague, 2009.
[54] P. Giannozzi, S. Baroni, N. Bonini, M. Calandra, R. Car, C. Cavazzoni, D. Ceresoli, G. L. Chiarotti, M. Cococcioni, I. Dabo, A. D. Corso, S. de Gironcoli, S. Fabris, G. Fratesi, R. Gebauer, U. Gerstmann, C. Gougoussis, A. Kokalj, M. Lazzeri, L. Martin-Samos, N. Marzari, F. Mauri, R. Mazzarello, S. Paolini, A. Pasquarello, L. Paulatto, C. Sbraccia, S. Scandolo, G. Sclauzero, A. P. Seitsonen, A. Smogunov, P. Umari, and R. M. Wentzcovitch1, J. Phys.: Condens. Matter **21**, 395502 (2009), URL http://www.quantum-espresso.org.
[55] M. Fronzi, A. Soon, B. Delley, E. Traversa, and C. Stampfl, J. Chem. Phys. **131**, 104701 (2009).
[56] L. Gerward, J. S. Olsen, L. Petit, G. Vaitheeswaran, V. Kanchana, and A. Svanee, J. Alloys Compd. **400**, 56 (2005).
[57] S. Duclos, Y. Vohra, A. Ruoff, A. Jayaraman, and G. Espinosa, Phys. Rev. B **38**, 7755 (1988).
[58] L. Gerward and J. Olsen, Powder Diffr. **8**, 127 (1993).
[59] C. Kittel, *Introduction to Solid State Physics* (Wiley, New York, 1996).
[60] F. Šutara, M. Cabala, L. Sedláček, T. Skála, M. Škoda, V. Matolín, K. C. Prince, and V. Cháb, Thin Solid Films **516**, 6120 (2008).
[61] V. Matolín, J. Libra, I. Matolínová, V. Nehasil, L. Sedláček, and F. Šutara, Appl. Surf. Sci. **254**, 153 (2007).
[62] Z. Yang, Z. L. an Gaixia Luo, and K. Hermansson, Phys. Lett. A **369**, 132 (2007).
[63] Z. Yang, Z. Lu, and G. Luo, Phys. Rev. B **76**, 075421 (2007).
[64] M. F. Camellone, L. Szabová, and S. Fabris (unpublished).
[65] S. Colussi, A. Gayen, M. F. Camellone, M. Boaro, J. Llorca, S. Fabris, and A. Trovarelli, Angew. Chem. **48**, 8481 (2009).
[66] A. Soon, M. Todorova, B. Delley, and C. Stampfl, Phys. Rev. B **73**, 165424 (2006).
[67] Y. Chen, M.-H. Lee, and H. Wang, Surf. Sci. **602**, 1736 (2008).
[68] C. Zhang, A. Michaelides, D. A. King, and S. J. Jenkins, J. Am. Chem. Soc. **132**, 2175 (2010).
[69] J. A. Rodríguez, J. Evans, J. Graciani, J.-B. Park, P. Liu, J. Hrbek, and J. F. Sanz, J. Phys. Chem. C **113**, 7364 (2009).